Self-Assembly

International Edition: DOI: 10.1002/anie.201604553
German Edition: DOI: 10.1002/ange.201604553

Hierarchical Self-Assembly of 3D-Printed Lock-and-Key Colloids through Shape Recognition

*Thomas Tigges and Andreas Walther**

Abstract: *Progress in colloid self-assembly crucially depends on finding preparation methods for anisotropic particles with recognition motifs to facilitate the formation of superstructures. Here, we demonstrate for the first time that direct 3D laser writing can be used to fabricate uniform populations of anisotropic cone-shaped particles that are suitable for self-assembly through shape recognition. The driving force for the self-assembly of the colloidal particles into linear supracolloidal polymers are depletion forces. The resulting supracolloidal fibrils undergo hierarchical ordering and form nematic liquid-crystalline domains. Such a behavior could so far not be observed in the absence of an electric field. The study opens possibilities for using direct laser writing to prepare designed colloids on demand, and to study their self-assembly.*

In colloid science, the preparation of defined particles with spatially confined properties persists in being one of the key challenges that attracts substantial attention.[1] Although the preparation of "patchy" spherical particles has significantly advanced in recent years, methods for preparing shape-anisotropic particles are still scarce.[2] Few approaches actually enable the preparation of shape-anisotropic particles. The self-assembly of block copolymers and directed epitaxial growth of inorganic nanoparticles are among the most promising methods for complex 3D objects, while classical photolithography allows 2D particles to be made.[3] Surface-anisotropic particles find application in the stabilization of interfaces, (bio)sensing, and self-propulsion as well as drug and cell delivery.[4]

Moreover, colloids at the mesoscale are of interest for fundamental studies, because direct in situ real-space and real-time imaging by optical microscopy allows for a deep understanding of self-assembly processes and collective phenomena. This is of profound importance to facilitate the understanding of similar processes at the nanoscale, where such processes can often only be observed ex situ.[5]

Many attempts to assemble colloidal particles utilize external fields, but an intriguing intrinsic property of anisotropic colloids is their propensity to spontaneously self-assemble under defined conditions to yield assemblies of high complexity.[6] Although there are valuable experimental approaches for the preparation of complex colloids, the exploration of superstructures and phase diagrams remains an experimental challenge, but it has been elegantly addressed by simulations.[7] In fact, simulations at present outrun experimental studies, as the freedom in the design of the particle geometry and surface patch distribution is basically unlimited in silico, while synthetic techniques need to catch up in terms of the complexity of accessible particle shapes.

Various driving forces have been implemented to guide the self-assembly of surface-anisotropic particles, such as confined hydrophobic interactions, selective chemical functionalization, metal complexation, and DNA recognition.[8] Sacanna and co-workers developed a method to self-assemble anisotropic particles by shape recognition, denoted "lock-and-key colloids". Therein, the structural anisotropy paired with a complementary shape enables controlled assembly. By introducing depletion interactions between the particles through the addition of a non-adsorbing polymer, the system maximizes its entropy by matching the lock-and-key pairs to obtain well-defined structures.[9] Even though the reported structures offer different possibilities by utilizing different lock-and-key pairs, the system still lacks the freedom in terms of particle design to prepare de novo designed self-assembling system on demand. Furthermore, larger self-assembled superstructures such as colloidal polymers or their higher level assemblies could not be obtained.

A convenient way to generate nano- to microstructures with high precision is direct 3D laser writing (DLW) with a confocal microscopy setup for controlled cross-linking of a resin through two-photon lithography. This technique has been used to create complex surface topologies for biological studies and optical metamaterials.[10] It was also recently used to prepare helical microcarriers.[11]

Herein, we go beyond surface-bound microstructures and single microcarriers and show that 3D-DLW gives new levels of design freedom for the self-assembly of particle systems. We design cone-shaped colloids suitable for homo- and coassembly that are small enough to operate as Brownian system. We further demonstrate their hierarchical self-assembly into directional supracolloidal fibers and their higher level organization into nematic domains. Furthermore, we present an approach for tailored coassemblies and break the directionality of the supracolloidal fibers by using symmetric double-cone particles. The overall strategy opens new and generic avenues to study the fundamental self-assembly behavior of designed 3D particle systems.

We designed by CAD software a self-complementary, cone-shaped particle geometry with a diameter of 4.5 μm and a height of 2.5 μm to act as the anisotropic colloid (Figure 1 a). The cone shape is a beneficial geometry when targeting shape recognition based on depletion interactions as the driving force, because the perfect insertion of one cone into another

[*] T. Tigges, Dr. A. Walther
DWI—Leibniz-Institute for Interactive Materials
Forckenbeckstrasse 50, 52074 Aachen (Germany)
E-mail: walther@dwi.rwth-aachen.de

Supporting information for this article can be found under: http://dx.doi.org/10.1002/anie.201604553.

 © 2016 Wiley-VCH Verlag GmbH & Co. KGaA, Weinheim

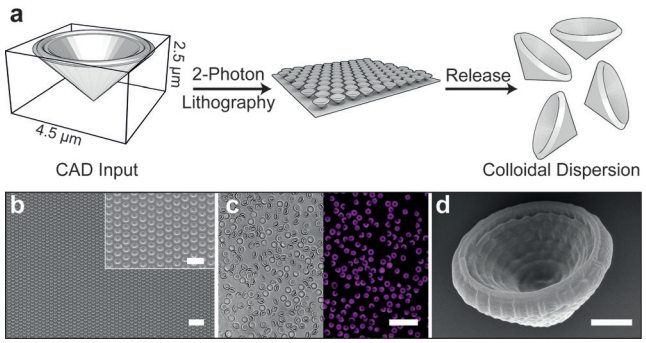

Figure 1. Particle design and DLW. a) Schematic representation of the particle geometry. The particle was designed using CAD software and generated as an array by DLW. The particles were released into aqueous solution containing 1% Pluronic F127 by scratching the substrate with a scalpel. b) SEM image of a 3D-written hexagonal array of cone particles. c) CLSM image of a dispersion of particles after release (left: bright field, right: fluorescence). d) Close-up SEM image of a single cone. Scale bars are 20 μm in (b) and (c) [inset in (b): 10 μm] and 1 μm in (d).

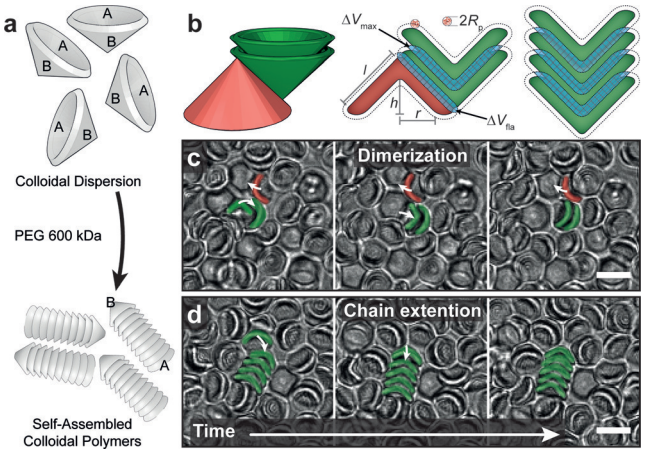

Figure 2. Self-assembly of cone-shaped DLW colloids driven by shape recognition through depletion interactions. a) Addition of PEG (600 kDa) triggers self-assembly of A-B-type colloids. b) Geometric rationalization of depletion interactions: The 3D schematic diagram shows cone-type particles stacked through shape recognition (green) against a non-adsorbed particle at the outer surface (red). The reduction in free energy is determined by the overlapping depletion volume ΔV (hatched) and reaches its maximum (ΔV_{max}) when the particles are stacked. c) CLSM snapshots during dimerization of particles (see Video 1 in the Supporting Information). Selectivity occurs through shape recognition; the green particle inserts into the cavity, while the red particle at the outer surface is repelled. d) Chain elongation at the tip of a tetramer. Scale bars are 5 μm.

provides a large reduction in free energy, as opposed to undesirable, nondirectional interactions of the particles in a side-by-side fashion, or with a substrate (Figure 2).

After DLW, the anisometric colloids are released from the substrate by immersion into an aqueous solution of 1 wt% Pluronic F127 and scratching the substrate with a scalpel or sonication (Figure 1b–d). The presence of the non-ionic tenside allows for a stable colloidal dispersion. As expected, the highly developed DLW process results in particles that are uniform, with an average diameter of (4.4 ± 0.1) μm and a height of (2.4 ± 0.1) μm, as determined by scanning electron microscopy (SEM) and confocal laser scanning microscopy (CLSM). The particle autofluorescence for characterization by CLSM is provided by the photoresist, which contains a photosensitizer to facilitate the two-photon absorption needed for the DLW. After preparation, the particles disperse in the aqueous surfactant solution and show slight sedimentation as a result of the higher density. This is beneficial, as it allows their self-assembly to be observed at high local concentration in the vicinity of a glass slide.

We chose depletion interactions to trigger the self-assembly of the colloids by adding non-adsorbing polyethylene glycol (PEG, 600 kDa) as a depletant. Depletion interactions provide short-range attraction between the colloids (Figure 2a) and are caused by the reduction in the free energy ΔF_d according to Equation (1).

$$\Delta F_d \approx k_b T n_p \Delta V \tag{1}$$

Each cone particle is surrounded by a depletion volume V that cannot be entered by the center of mass of the polymer and is thus defined by the polymer radius R_p. Accordingly, if two surfaces come closer than R_p, their excluded volumes overlap, as defined by the quantity ΔV. This increases the volume which is accessible by the depletant. Consequently, the entropy of the system rises and the free energy is decreased by ΔF_d. At a constant temperature T, the driving force is a function of the number of depletant molecules n_p, thus allowing the attractive force to be controlled by adjusting the concentration. Clearly, the addition of insufficient amounts of depletant keeps the whole dispersion disassembled, whereas an excess leads to irreversible clustering without proper shape recognition (see Figure S1 in the Supporting Information). However, at a specific concentration of the depletant, it is possible to arrive at a thermodynamic situation close to equilibrium, where shape recognition occurs, and irreversible clustering can be prevented.

The selectivity for shape recognition can be rationalized as follows. An estimation of the difference in ΔF_d between a stacked (shape recognition) and an associated (irregular) case can be drawn by comparing the overlapping depletion volumes for perfect shape recognition ΔV_{sr} versus full-line association of particles along their outside ΔV_{fla}. Since $\Delta F_d \propto \Delta V$ (at constant T and n_p), Equation 2 can be used to estimate the energy difference.

$$\frac{\Delta F_{d,sr}}{\Delta F_{d,fla}} = \frac{\Delta V_{sr}}{\Delta V_{fla}} \tag{2}$$

ΔV_{sr} can be calculated for the perfectly stacked case by considering the depletion volume at the inner cone surface with an inwardly oriented volume having a thickness equal to the polymer diameter $2R_p$, according to Equation (3). The parameter r denotes the inner radius and h the height (Figure 2).

$$\Delta V_{sr} = \frac{\pi}{3}[r^2 h - (r - 2R_p)^2 (h - 2R_p)] \tag{3}$$

© 2016 Wiley-VCH Verlag GmbH & Co. KGaA, Weinheim

Further details of the geometrical model can be found in the Supporting Information (Figure 2). The radius of the polymer R_p (ca. 56 nm) can be derived from the radius of gyration (see the Supporting Information).[12]

The side-by-side associated case has a maximum contact area when two particles attach along a full exterior contact line with a maximum length of 2.5 μm (Figure 2b). The corresponding overlapping depletion volume of both cones along this line ΔV_{fla} can be estimated using a cylinder with the length of that line l and the radius of the depletant R_p [Eq. (4)].

$$\Delta V_{fla} = \pi R_p^2 l \tag{4}$$

A comparison of the values for perfect cone/cone stacking versus irregular side-by-side association along a contact line leads to a considerable energetic preference for the shape-recognition with $\Delta V_{sr} \approx 75\,\Delta V_{fla}$. As a consequence of the curved outer surface, any other exterior association will have a smaller depletion volume ΔV compared to the perfect full-line association, and hence is much more unlikely ($\Delta V \ll \Delta V_{fla} \ll \Delta V_{sr}$; Figure 2b). In conclusion, the maximum overlapping depletion volume is reached when two particles are properly stacked through cone/cone shape recognition.

This energetic difference manifests in correct shape recognition and the first assemblies can be observed a few minutes after addition of the depletant (0.7 g L^{-1}). The initially formed dimers (green) progress into oligomers, while all other configurations do not lead to association (Figure 2c,d, as well as Video 1 in the Supporting Information). Hence, direct imaging reveals that shape recognition mediated supracolloidal polymerization is successfully controlled by the shape anisotropy, finally yielding supracolloidal fibrils with lengths exceeding 40 particles (Figure 3a,b). Importantly, this process does not require an external field, but is solely driven by controlled short-range forces in a Brownian system.

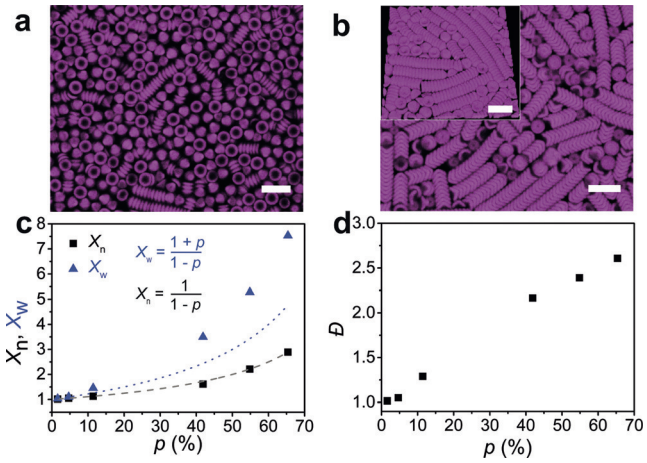

Figure 3. Characteristics of the supracolloidal polymerization. a, b) CLSM images after 48 h and 144 h, respectively. The inset shows a 3D representation of the hierarchical nematic assembly. Scale bars are 10 μm. c, d) Development of X_n, X_w, and Đ with the degree of polymerization p.

Similar to a classical polyaddition, we wanted to know to what extent the system can be understood by Carothers modeling.[8d,13] Therefore, we monitored the fibril length and conversion during the self-assembly process by statistical analysis of the CLSM images (Figure 3). When defining the particles as heterobifunctional monomers with the cavity and the tip representing the functions A and B, respectively, the extent of the reaction p_i can be expressed as Equation (5), with $n_{i,0}$ being the initial number of functional groups and n_i the number of reacted functional groups. The number- and weight-average degrees of polymerization (X_n and X_w) and the dispersity Đ are defined by Equation (6), where X_i is the number of particles in a polymer with length i, and N_i is the number of fibrils containing a certain number of particles.

$$p_i = \frac{n_{i,0} - n_i}{n_{i,0}} \tag{5}$$

$$X_n = \frac{\sum X_i N_i}{\sum N_i};\; X_w = \frac{\sum X_i^2 N_i}{\sum X_i N_i};\; Đ = \frac{X_w}{X_n} \tag{6}$$

Not surprisingly, very high X_n values can only be reached at high conversion, similar to what is known from classical step-growth polymerization. Accordingly, X_n proceeds to about 3 at 65 % conversion. Remarkably, X_n evolves in good agreement to step-growth reactions and can be fitted using the appropriate equation [Figure 3c, $X_n = 1/(1-p)$]. In contrast, X_w evolves faster than expected from the corresponding Carothers relationship ($X_w = (1+p)/(1-p)$). This discrepancy can be explained by the confinement of particles in the condensed 2D phase as well as the alignment of parallel chains, which restricts the rotation of the particles and guides the growth of already existing chains. The differences between X_w and X_n also lead to Đ values larger than predicted for perfect step-growth reactions (Figure 3d).

One of the most striking observations, beyond the formation of the supracolloidal chains, is the appearance of higher level 2D nematic liquid-crystalline domains that spontaneously occur without the assistance of an additional external field as the concentration and length of the supracolloidal fibrils increases (Figure 4). To the best of our knowledge, such a behavior could previously only be observed in string-forming self-assemblies upon directing them with an external field.[6b,14]

CLSM imaging of the resulting assemblies allows quantitative analysis of the periodicities of the self-assembled structures on different length scales by fast Fourier transformation (FFT) and gray-scale analysis (Figure 4a). The FFT shows two periodicities reminiscent, on the one hand, of the short-range order of the cones inside the supracolloidal fibrils and, on the other hand, originating from the lateral packing of the fibrils next to each other. The longer periodicity in the FFT p_1 corresponds to the d-spacing between individual particles in the self-assembled structures and can be calculated to be 1.3 μm, which is corroborated by the (1.3 ± 0.1) μm spacing determined by gray-scale analysis. The characteristic spacing between the supracolloidal chains can be deduced from the shorter spacing p_2 in the FFT to be 4.6 μm. Correlating this length scale with the diameter of the

 © 2016 Wiley-VCH Verlag GmbH & Co. KGaA, Weinheim

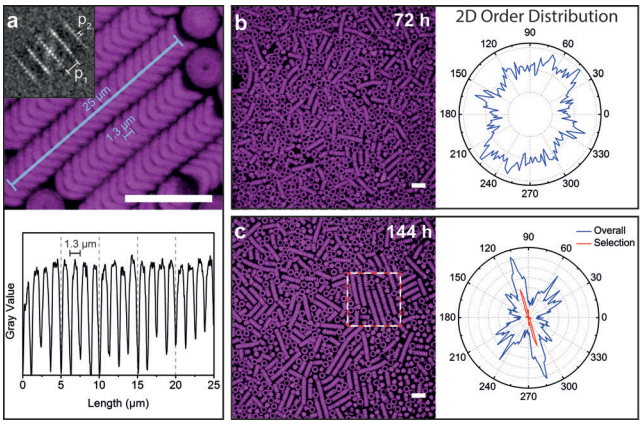

Figure 4. Hierarchical self-assembly. a) Top: CLSM image of self-assembled supracolloidal fibrils and FFT image (inset). The large periodicity p_1 indicates high local order between the particles within one fibril, while the small periodicity p_2 represents the long-range order of the fibrils. Bottom: Gray-scale analysis with an average periodicity of (1.3 ± 0.1) µm. b,c) CLSM images of self-assembled fibrils after 72 h and 144 h, respectively, and the corresponding radial 2D order distribution. The red graph in (c) illustrates the order in a single domain. Scale bars are 10 µm.

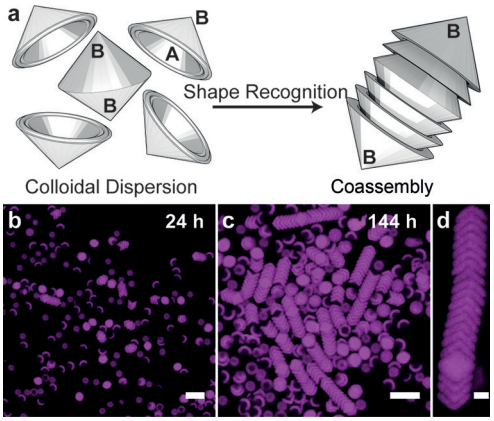

Figure 5. Coassembly. a) Illustration of the coassembly of a binary colloidal dispersion with complementary shape. The functionality of the A-B-type monomer is inverted when coassembled with the B-B-type monomer. b,c) CLSM micrographs of a binary colloidal dispersion after 24 h and 144 h, respectively. d) The close-up shows the coassembly around a central double cone. Scale bars are 10 µm in (b) and (c), and 2 µm in (d).

cones after 3D-DLW (ca. 4.4 µm) leads to an interchain gap of around 0.2 µm. Hence, the high particle order in the colloidal fibrils emphasizes the attraction between the particles through shape-recognition, while the larger interchain distance points to the absence of depletion interactions between the fibers (see Video 2 in the Supporting Information).

Further analysis of the development of the nematic, liquid-crystalline domains can be done by statistical image analysis of the 2D order parameter.[15] This is based on a parameterization of the images and by assigning vectors to the segments of the supracolloidal chains (single particles are ignored in the process). Whereas perfectly oriented samples show a single peak along one direction/angle, a plot of the 2D order parameter distribution of naturally occurring fibers shows a perfect circle both for a completely random orientation of all fibers and also for sufficiently large images of nematic domains with an overall evenly distributed orientation of the directors of the individual domains. Consequently, to obtain information on the order of fibrils in a nematic domain, an adequately small section is required, where overall randomization does not overcompensate local order.

Comparison of the order distribution in sections of the sample after 72 h and 144 h reveals a significant increase in 2D order at higher reaction times (Figure 4b,c). The plot starts to exhibit sharp peaks, which represent highly ordered domains inside the phase (Figure 4c). A further localized analysis of a section (red and white), shows the high order obtained in a single liquid-crystalline domain with nematic texture. While the system slows down in terms of progressing to even higher order, it will be interesting to understand whether higher order can be fostered by addition of active particles or using external directors.

The next challenge beyond homogeneous self-assembly of a single particle system is to approach coassembling systems with several different types of particles.[13,16] Although this has been established for bulk phases of simple spherical particles, it is a profound challenge for anisometric objects, in particular when targeting shape recognition as a driving force, where classical particle synthesis techniques reach their limits.[17] The 3D DLW process offers great flexibility and we focused on breaking the directionality of the self-assembled structures by coassembly with double-cone particles. The designed double cones have identical lateral dimensions as the basic cones, but present two identical binding sites for "face-selective growth", and correspond to a homobifunctional monomer of the B-B type.

To showcase this approach, we add 5 % of the B-B double cone particles to the system. This leads to a concurrent growth of free A-B chains with a single directionality, and A-B/B-B/B-A coassemblies with a two-faced directionality. Clearly, as the reaction progresses, the structures can merge and form long homobifunctional fibrils. This process can be followed by CLSM (Figure 5). Coassembly already takes place at early stages of the reaction (Figure 5b), which indicates a similar reactivity of both particles and a smooth "copolymerization". Subsequently, the chains elongate and display the two-sided direction (Figure 5c,d).

Although this type of coassembly gives a first impression of the principle feasibility, it is clear that changing the shape and functionality can be used to target more complex coassembling systems, for example, encoding branching points or defined chain stoppers. Furthermore, bifunctional coassemblies showcase the initial step for sequence control, which itself could be used to obtain superstructures with even higher definition and encoded lateral dimensions of the resulting structure.

In conclusion, we have presented a versatile approach for the precise design of 3D colloids that are able to self-assemble into defined superstructures without the need for external fields. The key factors are identifying and defining shapes that allow for shape recognition through well-balanced depletion

 © 2016 Wiley-VCH Verlag GmbH & Co. KGaA, Weinheim

interactions. Although we focused on the assembly of linear chains and discovered pathways to hierarchical structures with liquid-crystalline order, we believe the concept to be generic and applicable to the generation of a multitude of programmable colloidal assemblies through adjustment of the shape of the initial building block. We further showed that coassembly is possible by combining colloids with matched shape recognition and tuned functionality. We believe that the direct in situ observation of complex colloids will help to shed light on the self-assembly behavior of shape-anisometric nanoparticles, which can often only be observed ex situ.

The next challenges are to diversify the shape-recognition motifs and understand coassembling systems of higher complexity, be it isolated sequences and clusters, or self-sorting systems of orthogonally self-assembling species. This would lead to systems with highly selective and programmable functionalities, which until now have only been possible by utilizing expensive and preparatively challenging DNA functionalization as a recognition motif on patchy colloids.[18]

Looking to the future, combinations of orthogonally self-assembling motifs and defined branching points could facilitate true 3D self-assembly, and it will be interesting to identify new types of self-assembled optical materials based on unusual packings for photonic and metamaterial application.[19]

Acknowledgements

We thank the DFG for financial support in the framework of the SFB 985 C4 project. This work was performed in part at the Center for Chemical Polymer Technology, supported by the EU and the state of North Rhine-Westphalia (Grant No. EFRE 30 00 883 02).

Keywords: colloids · depletion interactions · direct laser writing · self-assembly · two-photon lithography

How to cite: *Angew. Chem. Int. Ed.* **2016**, *55*, 11261 – 11265
Angew. Chem. **2016**, *128*, 11429 – 11434

[1] A. Walther, A. H. E. Müller, *Chem. Rev.* **2013**, *113*, 5194 – 5261.
[2] a) A. B. Pawar, I. Kretzschmar, *Langmuir* **2008**, *24*, 355 – 358; b) L. Feng, R. Dreyfus, R. Sha, N. C. Seeman, P. M. Chaikin, *Adv. Mater.* **2013**, *25*, 2779 – 2783.
[3] a) P. A. Rupar, L. Chabanne, M. A. Winnik, I. Manners, *Science* **2012**, *337*, 559 – 562; b) H.-H. Jeong, A. G. Mark, T.-C. Lee, K. Son, W. Chen, M. Alarcón-Correa, I. Kim, G. Schütz, P. Fischer, *Adv. Sci.* **2015**, *2*, 1500016; c) A. H. Gröschel, F. H. Schacher, H. Schmalz, O. V. Borisov, E. B. Zhulina, A. Walther, A. H. E. Müller, *Nat. Commun.* **2012**, *3*, 710; d) C. J. Hernandez, T. G. Mason, *J. Phys. Chem. C* **2007**, *111*, 4477 – 4480.
[4] a) J. Palacci, S. Sacanna, A. P. Steinberg, D. J. Pine, P. M. Chaikin, *Science* **2013**, *339*, 936 – 940; b) Y. Su, Y. Ge, L. Liu, L. Zhang, M. Liu, Y. Sun, H. Zhang, B. Dong, *ACS Appl. Mater. Interfaces* **2016**, *8*, 4250 – 4257; c) M. Medina-Sánchez, L. Schwarz, A. K. Meyer, F. Hebenstreit, O. G. Schmidt, *Nano Lett.* **2016**, *16*, 555 – 561; d) A. Walther, K. Matussek, A. H. E. Müller, *ACS Nano* **2008**, *2*, 1167 – 1178.
[5] G. van Anders, N. K. Ahmed, R. Smith, M. Engel, S. C. Glotzer, *ACS Nano* **2014**, *8*, 931 – 940.
[6] a) B. Bharti, O. D. Velev, *Langmuir* **2015**, *31*, 7897 – 7908; b) A. A. Shah, B. Schultz, W. Zhang, S. C. Glotzer, M. J. Solomon, *Nat. Mater.* **2015**, *14*, 117 – 124.
[7] a) G. A. Chapela, O. Guzman, J. A. Martinez-Gonzalez, P. Diaz-Leyva, J. Quintana-H, *Soft Matter* **2014**, *10*, 9167 – 9176; b) Z. Zhang, S. C. Glotzer, *Nano Lett.* **2004**, *4*, 1407 – 1413.
[8] a) T. Tigges, D. Hoenders, A. Walther, *Small* **2015**, *11*, 4540 – 4548; b) Q. Chen, S. C. Bae, S. Granick, *Nature* **2011**, *469*, 381 – 384; c) Y. Wang, A. D. Hollingsworth, S. K. Yang, S. Patel, D. J. Pine, M. Weck, *J. Am. Chem. Soc.* **2013**, *135*, 14064 – 14067; d) K. Liu, Z. Nie, N. Zhao, W. Li, M. Rubinstein, E. Kumacheva, *Science* **2010**, *329*, 197 – 200.
[9] a) L. Colón-Meléndez, D. J. Beltran-Villegas, G. van Anders, J. Liu, M. Spellings, S. Sacanna, D. J. Pine, S. C. Glotzer, R. G. Larson, M. J. Solomon, *J. Chem. Phys.* **2015**, *142*, 174909; b) S. Sacanna, W. T. M. Irvine, P. M. Chaikin, D. J. Pine, *Nature* **2010**, *464*, 575 – 578.
[10] a) T. K. Claus, B. Richter, V. Hahn, A. Welle, S. Kayser, M. Wegener, M. Bastmeyer, G. Delaittre, C. Barner-Kowollik, *Angew. Chem. Int. Ed.* **2016**, *55*, 3817 – 3822; *Angew. Chem.* **2016**, *128*, 3882 – 3887; b) F. Klein, B. Richter, T. Striebel, C. M. Franz, G. von Freymann, M. Wegener, M. Bastmeyer, *Adv. Mater.* **2011**, *23*, 1341 – 1345; c) J. K. Gansel, M. Thiel, M. S. Rill, M. Decker, K. Bade, V. Saile, G. von Freymann, S. Linden, M. Wegener, *Science* **2009**, *325*, 1513 – 1515.
[11] S. Tottori, L. Zhang, F. Qiu, K. K. Krawczyk, A. Franco-Obregón, B. J. Nelson, *Adv. Mater.* **2012**, *24*, 811 – 816.
[12] K. Devanand, J. C. Selser, *Macromolecules* **1991**, *24*, 5943 – 5947.
[13] A. H. Gröschel, A. Walther, T. I. Löbling, F. H. Schacher, H. Schmalz, A. H. E. Müller, *Nature* **2013**, *503*, 247 – 251.
[14] a) M. Kamp, N. A. Elbers, T. Troppenz, A. Imhof, M. Dijkstra, R. van Roij, A. van Blaaderen, *Chem. Mater.* **2016**, *28*, 1040 – 1048; b) H. R. Vutukuri, A. F. Demirörs, B. Peng, P. D. J. van Oostrum, A. Imhof, A. van Blaaderen, *Angew. Chem. Int. Ed.* **2012**, *51*, 11249 – 11253; *Angew. Chem.* **2012**, *124*, 11411 – 11415.
[15] I. Usov, R. Mezzenga, *Macromolecules* **2015**, *48*, 1269 – 1280.
[16] A. Schreiber, M. C. Huber, H. Cölfen, S. M. Schiller, *Nat. Commun.* **2015**, *6*, 6705.
[17] T. Paik, B. T. Diroll, C. R. Kagan, C. B. Murray, *J. Am. Chem. Soc.* **2015**, *137*, 6662 – 6669.
[18] H. Qi, M. Ghodousi, Y. Du, C. Grun, H. Bae, P. Yin, A. Khademhosseini, *Nat. Commun.* **2013**, *4*, 2275.
[19] a) T. Bückmann, M. Thiel, M. Kadic, R. Schittny, M. Wegener, *Nat. Commun.* **2014**, *5*, 4130; b) J. K. Gansel, M. Latzel, A. Frölich, J. Kaschke, M. Thiel, M. Wegener, *Appl. Phys. Lett.* **2012**, *100*, 101109.

Received: May 10, 2016
Published online: July 28, 2016

 © 2016 Wiley-VCH Verlag GmbH & Co. KGaA, Weinheim